Quantum Electronics **51** (1) 38–42 (2021)

https://doi.org/10.1070/QEL17479

Optical coherence tomograph for non-invasive examination of the human middle ear

P.A. Shilyagin, A.A. Novozhilov, T.E. Abubakirov, A.L. Dilenyan, A.V. Shakhov, A.A. Moiseev, D.A. Terpelov, S.Yu. Ksenofontov, V.A. Matkivsky, V.M. Gelikonov, G.V. Gelikonov

Abstract. **The paper describes the design of an optical coherence tomograph adapted for studying the state of the tympanic cavity of the human middle ear. We present the images obtained by the method of optical coherence tomography, which are characteristic of the norm and of the case of pathology – otitis media with effusion.**

Keywords: *optical coherence tomography, otitis media with effusion, non-invasive diagnostics, medical biophotonics.*

1. Introduction

Otitis media with effusion (OME) is a non-purulent disease of the middle ear, which is characterised by the accumulation of fluid (exudate) in the tympanic cavity, accompanied by a restriction of the mobility of the tympanic membrane. The clinical picture of OME is characterised by the absence of pain and signs of active inflammation, most often by moderate hearing loss and noise in the ear. The long course of OME and the lack of adequate treatment can lead to the development of complications, including purulent ones that require complex sanitising and reconstructive interventions. Up to 11% of OME cases are attended with violations of auditory nerve operation and the development of sensorineural hearing loss [1]. Even a slight hearing loss in children can lead to impaired speech and thinking as well as affect emotional status. This confirms the relevance of the problem of diagnosis and treatment of OME and brings this pathology to the fore among middle ear diseases both in our country and around the world.

The smoothness of clinical manifestations and a wide variability of otoscopic signs often make it difficult to diagnose OME at a regular appointment with an otolaryngologist (ENT doctor). Standard otoscopy has a low sensitivity (74%–87%) and specificity (60%–74%) in the diagnosis of OME [2–4]. At present, objective diagnostics of OME requires the participation of a second narrow specialist – an audiologist – and a set of complex equipment accommodated in a special soundproof room. Audiometry is supplemented by the impedance measurement, which includes acoustic reflexometry, tympanometry [5]. The sensitivity of tympanometry is 85.5% and the specificity is 72% [5, 6]. Tympanometry results indicate that the mobility of the eardrum is restricted, most often due to the presence of fluid in the tympanic cavity, but other reasons for limited mobility of the middle ear are also possible.

Optical coherence tomography (OCT) permits visualising the existence of a scattering medium behind the eardrum, which makes possible direct liquid detection in the tympanic cavity [7–9]. In this case, the use of near-IR radiation makes the procedure non-invasive and permits obviating the introduction of conductive media into the external auditory canal, as in ultrasound studies [10, 11]. The main method for identifying clinically significant information obtained using OCT is a visual examination of the resultant structural image, which gives the overall sensitivity and specificity of the method at 91% and 90%, respectively, with the consent of respondents at a level of 87%, according to research performed in 2019 [12]. Apart from the visual image examination, techniques for the numerical analysis of OCT data were also proposed, which made it possible to estimate the mobility of scatterers in the exudate, which in turn makes it possible to distantly estimate its viscosity [9, 13, 14] and thereby select the optimal treatment tactics.

The present paper describes an optical coherence tomograph intended for diagnosing the diseases of the middle ear and, primarily, the OME.

2. OCT design adapted for otoscopic examinations

Otoscopic probe. The structural features of the human hearing apparatus exclude the wide use of contact probes and also impose significant restrictions on the possibility of organising wide-field scanning. In the development of the probe, special emphasis was placed on ensuring the sterility of the performed studies by combining the scanning device and standard ear funnel used in routine otoscopic practice. This favourably distinguishes the device we have developed from the one described in Refs [12, 15] and its commercial implementation TOMi Scope (PhotoniCare, Inc., USA) (which received FDA approval at the end of 2019), which uses custom-made ear specula.

The schematic optical diagram of the scanning device is shown in Fig. 1. The collimated probe beam is deflected by a

P.A. Shilyagin, A.A. Moiseev, D.A. Terpelov, S.Yu. Ksenofontov, V.A. Matkivsky, V.M. Gelikonov, G.V. Gelikonov Institute of Applied Physics, Russian Academy of Sciences, ul. Ul'yanova 46, 603155 Nizhny Novgorod, Russia; e-mail: paulo-s@mail.ru;
A.A. Novozhilov, T.E. Abubakirov, A.L. Dilenyan Institute of Applied Physics, Russian Academy of Sciences, ul. Ul'yanova 46, 603155 Nizhny Novgorod, Russia; Privolzhsky District Medical Centre of the Federal Medical and Biological Agency of Russia, Nizhnevolzhskaya nab. 2, 603001 Nizhny Novgorod, Russia;
A.V. Shakhov Institute of Applied Physics, Russian Academy of Sciences, ul. Ul'yanova 46, 603155 Nizhny Novgorod, Russia; Privolzhsky Research Medical University of the Ministry of Health of Russia, pl. Minina i Pozharskogo 10/1, 603005 Nizhny Novgorod, Russia

Received 10 November 2020
Kvantovaya Elektronika **51** (1) 38–42 (2021)
Translated by E.N. Ragozin

scanning mirror located in plane *1*. The telecentric focusing group (*2*) translates the angular distribution of radiation in plane *1*, which is located in the front focal plane of the group, into the spatial distribution in its rear focal plane (*1′*). The paired lens system (*4*) transfers the image from plane *1′* to plane *7* located inside the object of study with a 1.4-fold magnification. The transfer of the image plane beyond the rear focal plane of the lens system (*4*) permits scanning through a limited aperture hole without losing the scanning range. The minimal cross sections (apertures) of both channels (OCT and video recording) are located in plane *6*, which permits us to accommodate a video channel illumination system in it. The system consists of six circularly arranged white light LEDs, which are mounted on a metal heat sink and produce a quasi-uniform illumination field in the observation plane.

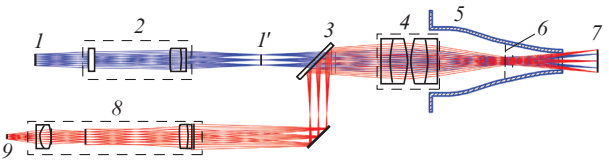

Figure 1. Optical configuration of the scanning device: (*1*, *1′*) scanning mirror planes of the OCT channel; (*2*) telecentric focusing group; (*3*) dichroic mirror; (*4*) scanning lens group; (*5*) removable standard ear funnel; (*6*) plane of the location of illumination diodes; (*7*) plane of probing radiation focusing; (*8*) camera lens; (*9*) CCD matrix plane.

To achieve flexible probe adjustment during pilot examinations, the position of the removable funnel (*5*) relative to the focus plane can vary within ±5 mm. This makes it possible to provide, if necessary, a partial focus of the probe in the wall of the external auditory canal, regardless of its gOMEetric length, and in turn makes it possible to examine the tympanic cavity with different anatomical features and in different age groups.

To effectively point the scanning device at the object under examination, the optical path provides for the placement of a CCD matrix (*9*), on which the scanning plane (*7*) is imaged in the visible wavelength range.

The introduction of a video channel into the optical configuration of the scanning device permits the OCT device to be supplemented with the function of a digital otoscope, which is also important for the clinical application of the device. A dichroic long-path mirror 69-874 (Edmund Optics) was used for spectral channel separation.

The base unit of OCT tomography. Structurally, the base unit is implemented according to a tandem interferometric scheme [16] (Fig. 2) with the use of flexible probes with isotropic optical fibre. The source of probing radiation was a superluminescent diode EXS210046-2 (Exalos, USA) with a centre wavelength of 1307 nm, a half-height spectrum width of 68 nm and an output radiation power up to 15 mW. To simplify the object search procedure during experimental testing, the length of the reference arm of the Michelson interferometer (*4*) (Fig. 2) could vary within ±5 mm. For a long waist length of the probe beam, this made it possible to use it for searching the position of the object under study with only a slight deterioration in the clarity of the images obtained.

Diffraction grating spectrometer T-1200-1310 (LightSmyth, USA) with a line density of 1200 lines mm^{-1} has

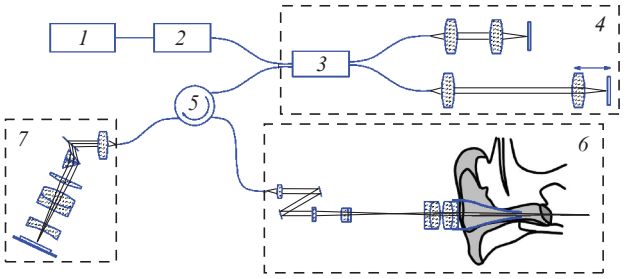

Figure 2. Optical configuration of the OCT base unit: (*1*) superluminescent diode; (*2*) optical isolator; (*3*) 3-dB coupler; (*4*) additional Michelson air interferometer; (*5*) optical circulator; (*6*) scanner (basic Fizeau interferometer); (*7*) spectrometer.

a recording bandwidth of 80 nm. Equidistancy correction of the registration of spectral components is carried out using a combined corrector [17] based on custom-made elements (Nanyang Jingliang Optical Technology Corp., China). The antireflection coating deposited by the manufacturer rules out the occurrence of polarisation anisotropy at corrector elements and provides for the integral transmittance up to 98% for the radiation of the target range. The focusing element is a plan-lens ($f = 103$ mm) of our own design with an extended aperture stop, which has minimal distortion (0.02% at the edge of the field of view). The optical spectrum of the sum of interfering waves is recorded using an SU-512LDB-1.7T1 linear photodetector array (Goodrich, USA). The bandwidth-limited spatial resolution of the base unit is 11 μm; the maximum range of imaging in depth in one frame is 3.2 mm.

In the recording images of the tympanic membrane, the sensitivity of the developed device (in signal-to-noise ratio) was 60 dB, which required special measures to exclude the influence of heterodyne artifacts characteristic of systems using multi-channel photodetector elements [18]. Although during the OCT examination of the tympanic cavity there is a possibility of contact between the side surface of the probe and the surface of the external auditory canal, which reduces the influence of involuntary displacements of the probe in the transverse direction, such contact can hardly prevent the appearance of displacements in the direction of optical sensing. The experimentally recorded displacements had a significant effect on the surface shape visualised in the three-dimensional scanning as well as on the possibility of extracting the corresponding information from the OCT data. In this connection, the software of the device provided for the suppression of micro-displacements of the probe relative to the object under examination [19, 20]. Furthermore, the software package of the device implements an algorithm that corrects the influence of fast motions characteristic of the target search procedure [21], which leads to the disappearance of the signal from the spectral OCT image under certain conditions. This procedure permits restoring the brightness of the OCT image in real time, which is especially important when using probes with a short working length, since the constant presence of a signal on the screen makes it possible not only to correctly assess the direction and speed of the probe motion, but also to avoid extremely undesirable contact of the probe tip with an extremely sensitive object – the eardrum.

In addition, the base unit provides the ability to change the hardware mode of research from three-dimensional to a mode that is essentially close to the M mode, in which scanning occurs in one plane without shifting along the second

coordinate. In this case, the difference from the M mode consists in that the displacement of the scanning plane nevertheless occurs, but at a speed many times lower than the displacement speed during 3D scanning. This allows us to consider up to 50 consecutive OCT images obtained in the mode we used as images from a single plane, and the full set of recorded data captures about 20 such image volumes, which significantly raises the probability of detecting single scatterers in this mode that are in the exudates in early formation stages.

3. Experimental testing of the OCT device

Figure 3 shows the external appearance of the device developed and tested in this work, which consists of an interferometric unit (*1*) and a scanner probe (*4*). Displayed on the front panel of the device are the drive (*2*) for changing the length of the reference arm and the toggle switch (*3*) for switching the operating modes of the device. Directly on the body of the scanner probe, there are couplings for fixing the replaceable otoscopic funnel (*6*) and adjusting the position of the funnel relative to the focus plane (*7*).

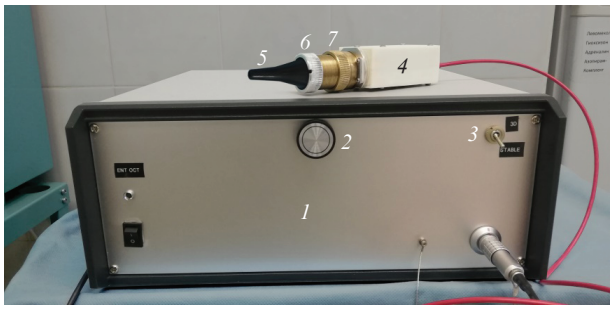

Figure 3. External view of the OCT device with an attached probe: (*1*) base (interferometric) unit; (*2*) drive for changing the length of the reference arm; (*3*) operating mode switch; (*4*) scanner probe; (*5*) replaceable standard ear funnel; (*6*) funnel mounting coupling; (*7*) coupling for adjusting the position of the funnel relative to the focal plane.

The developed tomograph was experimentally tested with the involvement of volunteers on the basis of the ENT Department of the Privolzhsky District Medical Centre of the Federal Medical and Biological Agency of Russia. The study was approved by the local Research Ethics Committee of the Volga Research Medical University of the Ministry of Health of Russia (Protocol No. 7 of 03.07.17).

Figure 4 shows the eardrum and tympanic cavity images of a healthy volunteer and of patients with a confirmed diagnosis of OME obtained using our developed device. In the image of the video channel (Fig. 4a), contour A highlights the area of OCT information acquisition. Since the stretched part of the eardrum is most important from the viewpoint of diagnostic information, the lower quadrants were mainly chosen for the examination.

Figures 4c and 4d show the images of the tympanic cavity in the case of confirmed OME. One can see that normally (Fig. 4b) the tympanic cavity does not contain traces of scatterers, except for regular structures of the middle ear that fall into the field of view of the device. By contrast, in the presence of exudate in varying degrees of development, identified in the volume of the tympanic cavity are single scatterers (Fig. 4c) or a uniformly scattering medium.

In the acute course of OME (56% of patients in the study group), exudate is a highly transparent liquid containing indi-

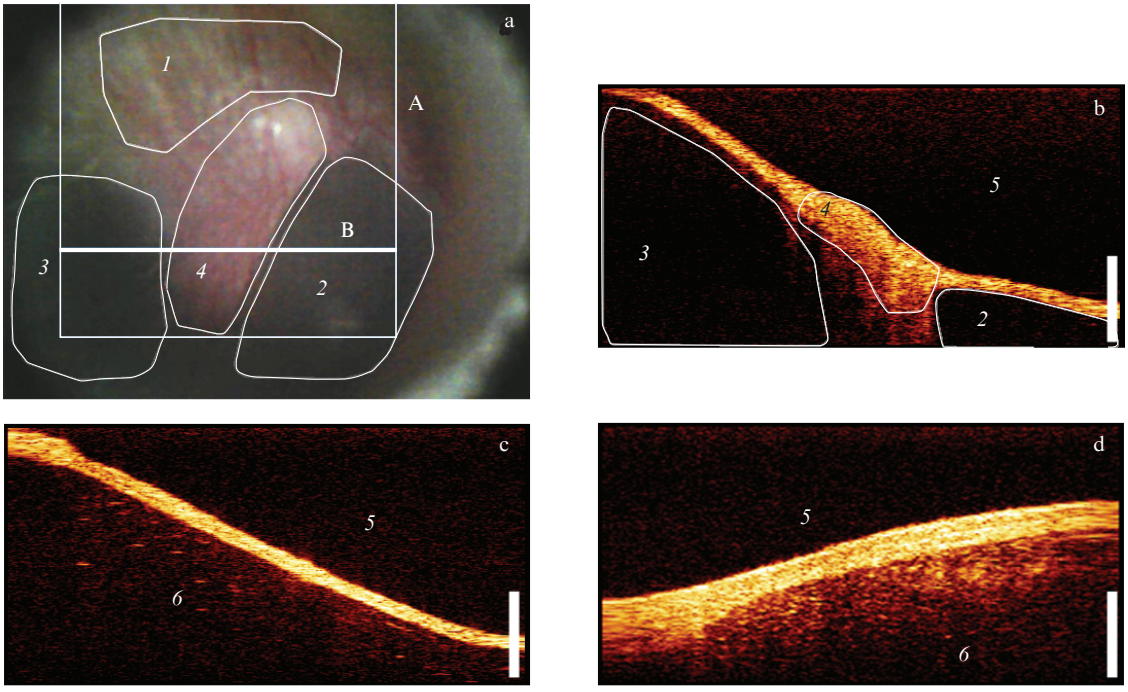

Figure 4. Images of the volunteer's tympanic cavity obtained using the video channel (a) and the OCT method (b), patients with early-stage acute OME with a fluid exudate (c), a patient with chronic OME with a high-viscosity effusion (d):
(*1*) non-stretched part of the tympanic membrane; (*2*) anterior-upper quadrant of the stretched part; (*3*) posterior-upper quadrant of the stretched part; (*4*) hammer handle; (*5*) external auditory canal; (*6*) tympanic cavity in the lower quadrants; (A) OCT-sensing area; (B) image plane of Fig. 4b. The bar height is 1 mm.

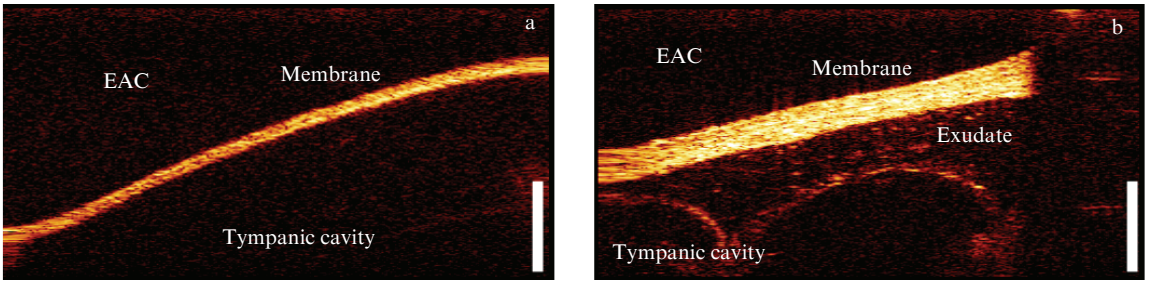

Figure 5. OCT-image of the tympanic membrane in normal (a) and in chronic OME (b); EAC is the external auditory canal. The bar height is 1 mm.

vidual inclusions of large scattering objects (fragments of the mucous membrane damaged by an acute inflammatory process, and cellular structures). For prolonged and chronic OME course (44% in the study group), the OCT image of the tympanic cavity is characterised by uniform scattering over the entire volume available for observation, while the average signal level in the image significantly exceeds the noise level. This pattern is explained by the dominant scattering of light from high-molecular structures – DNA fragments, protein structures, and glycopolysaccharides present in the exudate in significant amounts during the long course of the disease [12, 22].

Figure 4b shows a clinical example of an early course of OME. Discernible in the visual assessment of the OCT image is the structure of the tympanic membrane, as well as individual intense inclusions against the low-intensity exudate background. As a result of a small surgical intervention (limited to tympanostomy), a liquid effusion was obtained, a shunt was installed and medication was prescribed, which led to the patient's recovery.

Figure 5b shows a clinical example of a chronic prolonged course of OME. Discernible in the visual assessment of the OCT image is the structure of the eardrum; a high-intensity signal in the tympanic cavity in the form of a quasi-uniformly scattering structure is also seen. Surgical intervention (limited to bilateral tympanostomy: a similar pattern was observed for the second ear) was performed, a highly viscous effusion was obtained, shunts were installed, and medication was prescribed.

In total, the study group included 24 patients with OME (11 women and 13 men) between 22 and 76 years of age, who were advised surgical treatment – tympanostomy; 5 patients had a bilateral process (29 OME cases in all). After exudate evacuation, its viscosity was evaluated in patients of the study group.

Studies of clinical material [23] and analysis of literature data [12] allow a conclusion that it is possible to identify the state of exudate by statistical characteristics of the OCT image.

The second important result obtained in a clinical setting is related to the detection of a correspondence between the thickness of the tympanic membrane measured from OCT images and the clinical picture of the disease. The study of eardrum thickness analysed the results of an examination of 56 patients with OME aged 18 to 76 years; a total of 73 measurements were performed. The control group consisted of 28 patients without middle ear pathology, and 31 studies were performed.

The OCT-based measurement of the thickness of tympanic membrane was performed in its stretched part at the same distance from the fibrous ring and the place of attachment of the hammer in the line-of-sight zone. Quantitative analysis of the resultant OCT images was performed manually using the open-source ImageJ software. Statistical processing of the results revealed a statistically significant difference between the thickness of tympanic membrane in normal and in the presence of atrophic changes ($p < 0.001$), as well as when comparing the figures in normal and in chronic OME ($p < 0.001$).

4. Conclusions

The optical coherence tomography device developed in our work can be used in the routine practice of ENT specialists to study the state of the human middle ear and diagnose otitis media with effusion. The device allows an effective detection the presence of a scattering liquid behind the eardrum.

Studies of clinical material and analysis of literature data allow us to conclude that it is possible to identify the state of exudate by statistical characteristics of the OCT image.

Measurements of the distribution of the average value of the tympanic membrane thickness performed in the study group suggest that it is possible to determine the chronic or acute nature of the disease even in the absence of this information in the anamnesis.

Acknowledgements. In terms of development and clinical testing of the OCT device prototype, the work was supported by the Russian Science Foundation (Project No. 17-15-01507); in terms of improving the solutions used in the development and making a parallel video recording channel the work was performed in the framework of the state task of the IAP RAS (Project No. 0035-2019-0013).

References

1. Lambert M. *Am. Fam. Physician*, **94**, 747 (2016).
2. Kaleida P.H., Stool S.E. *Am. J. Dis. Child.*, **146**, 433 (1992).
3. Lee D.-H., Yeo S.-W. *J. Korean. Med. Sci.*, **19**, 739 (2004).
4. Harris P.K., Hutchinson K.M., Moravec J. *Am. J. Audiol.*, **14**, 3 (2005).
5. Taiji H., Kanzaki J. *Nippon Jibiinkoka Gakkai Kaiho*, **119**, 727 (2016).
6. Sharma K., Pannu M.S., Arora A., Sharma V. *Indian J. Otolaryngol. Head Neck Surg.*, **68,** 163 (2016).
7. Meller A., Shakhova M., Rilkin Y., Novozhilov A., Kirillin M., Shakhov A. *Photon. Lasers Medic.*, **3**, 323 (2014).
8. Novozhilov A.A., Shakhov A.V. *Folia Otorhinolaringol.*, **22**, 46 (2016).
9. Monroy G.L., Pande P., Shelton R.L., Nolan R.M., Spillman D.R. Jr., Porter R.G., et al. *J. Biophoton.*, **10**, 394 (2017).
10. Landry T.G., Rainsbury J.W., Adamson R.B., Bance M.L., Brown J.A. *Hearing Research*, **326**, 1 (2015).

11. Seth R., Discolo C.M., Palczewska G.M., Lewandowski J.J., Krakovitz P.R. *Am. J. Otolaryngol*., **34**, 44 (2013).
12. Preciado D., Nolan R.M., Joshi R., Krakovsky G.M., Zhang A., Pudik N.A., Kumar N.K., Shelton R.L., Boppart S.A., Bauman N.M. *Otolaryngol. Head Neck Surg*., **162**, 367 (2020).
13. Shilyagin P.A., Novozhilov A.A., Abubakirov T.E., Gelikonova V.G., Terpelov D.A., Matkivsky V.A., Gelikonov G.V., Shakhov A.V., Gelikonov V.M. *Laser Phys. Lett*., **15**, 096201 (2018).
14. Shilyagin P., Novozhilov A., Abubakirov T., Gelikonov G., Shakhov A., Gelikonov V. *Proc. SPIE*, **11078**, 11078_26 (2019).
15. Cho N.H., Lee S.H., Jung W., Jang J.H., Kim J. *J. Korean Med. Sci*., **30**, 328 (2015).
16. Gelikonov V.M., Gelikonov G.V., Shilyagin P.A. *Bull. Rus. Acad. Sci.: Phys*., **72**, 93 (2008) [*Izv. Ross. Akad. Nauk, Ser. Fiz*., **72**, 104 (2008)].
17. Shilyagin P.A., Ksenofontov S.Yu., Moiseev A.A., Terpelov D.A., Matkivskii V.A., Kasatkina I.V., Mamaev Yu.A., Gelikonov G.V., Gelikonov V.M. *Radiophys. Quantum Electron*., **60**, 769 (2018) [*Izv. Vyssh. Uchebn. Zaved. Radiofiz*., **60**, 859 (2017)].
18. Ksenofontov S.Yu., Terpelov D.A., Gelikonov G.V., Shilyagin P.A., Gelikonov V.M. *Radiophys. Quantum Electron*., **62**, 151 (2019) [*Izv. Vyssh. Uchebn. Zaved. Radiofiz*., **62**, 167 (2019)].
19. Gelikonov G.V., Ksenofontov S.Yu., Shilyagin P.A., Gelikonov V.M. *Radiophys. Quantum Electron*., **62**, 228 (2019) [*Izv. Vyssh. Uchebn. Zaved. Radiofiz*., **62**, 252 (2019)].
20. Ksenofontov S.Y., Shilyagin P.A., Terpelov D.A., Gelikonov V.M., Gelikonov G.V. *Fronti. Optoelectron*. (2020) (in press); https://doi.org/10.1007/s12200-019-0951-0.
21. Ksenofontov S.Y., Shilyagin P.A., Terpelov D.A., Novozhilov A.A., Gelikonov V.M., Gelikonov G.V. *Instrum. Experiment. Techniques*, **63**, 126 (2020).
22. Val S., Poley M., Anna K., Nino G., Brown K., Pérez-Losada M., Gordish-Dressman H., Preciado D. *Pediatr. Research*, **84**, 296 (2018).
23. Novozhilov A.A., Shilyagin P.A., Abubakirov T.E., Dilenyan A.L., Klimycheva M.B., Gelikonov G.V., Ksenofontov S.Yu., Gelikonov V.M., Shakhov A.V. *Vestn. Otorinolaringologii*, **85**, 16 (2020).